Dual-surface flexible THz Fano metasensor

Srivastava, Yogesh Kumar; Cong, Longqing; Singh, Ranjan

2017

Srivastava, Y. K., Cong, L., & Singh, R. (2017). Dual-surface flexible THz Fano metasensor. Applied Physics Letters, 111(20), 201101-.

https://hdl.handle.net/10356/86700

https://doi.org/10.1063/1.5000428

Dual-surface flexible THz Fano metasensor

Yogesh Kumar Srivastava,[1,2,a)] Longqing Cong,[1,2,a)] and Ranjan Singh[1,2,b)]
[1]*Division of Physics and Applied Physics, School of Physical and Mathematical Sciences, Nanyang Technological University, 21 Nanyang Link, Singapore 637371, Singapore*
[2]*Centre for Disruptive Photonic Technologies, The Photonics Institute, Nanyang Technological University, 50 Nanyang Avenue, Singapore 639798, Singapore*

(Received 16 August 2017; accepted 19 October 2017; published online 13 November 2017)

Sensing technologies based on terahertz waves have immense potential due to their non-destructive, transparent, and fingerprint spectral response of several materials that are opaque to other parts of the electromagnetic spectrum. Terahertz metasensors reported so far merely exploit the fringing electric field on the top of the subwavelength resonators. Here, we experimentally demonstrate an ultrathin flexible terahertz metamaterial sensor on a low refractive index substrate which enables sensing of analytes from the top and bottom surfaces of the metamaterial, opening up avenues for *dual-surface sensing* of analytes with fringing resonant fields on both front and rear sides of a metasurface. Since most of the real-world objects have 3D curvatures, the reported flexible metasensor with large mechanical strength and stability in free space would be an ideal platform for ultrasensitive sensing of dielectrics, chemicals, and biomolecules of extremely low concentrations with dual non-planar surfaces. *Published by AIP Publishing.*
https://doi.org/10.1063/1.5000428

In sharp contrast to label based sensors that detect the target with labelled molecules, label-free chemical and biological sensing modalities through optical approaches are undergoing a continued quest in developing enhanced sensitivity and stable sensing platforms.[1–4] Taking advantage of novel emergent chemical signatures has stimulated increasing interest in terahertz, infrared, and optical regimes, among which the terahertz (THz) wave reveals extraordinary advantages due to spectral fingerprint signatures of several materials that exist in the THz regime,[5] such as explosives, proteins, and DNA.[6,7] The precise response of materials in the THz spectrum has enabled commercial security inspection equipment instead of X-ray imaging that has ionizing and harmful characteristics due to extremely high photon energy.[8,9] Among different sensing platforms, metamaterials,[10–16] a periodic array of subwavelength sized resonators, have exhibited remarkable performance due to the strongly confined resonant energy in resonators so that the longer light-matter interaction time provides a better sensitivity for small volume of analytes. A variety of label-free refractometric sensing devices have been proposed by using plasmonic[3,4,17–20] and all-dielectric metamaterials[21,22] in different spectral ranges. However, most of the state-of-art sensors are based on rigid substrates for the ease of fabrication.[23–26] With the recent technological advancements in optoelectronic devices, flexible components are required in applications of displays, flexible cell phones, wearable devices, and biosensors.[27–30] The development of photonic sensors on flexible substrates has recently attracted a lot of attention[27,28,31–33] due to their practicality that mainly arises from the three dimensional curvature of most objects in our surroundings. Additionally, a typical configuration of a metamaterial sensor is to use the top metafilm surface with an optically thick substrate. Most of the previous sensing demonstrations were limited to using only the top surface that consisted of the metallic/dielectric resonator array.[34] The idea of utilizing the rear (bottom) surface of the substrate was not explored much since the resonantly enhanced fringing fields of the resonators on the top surface do not penetrate through the optically thick substrate to the rear surface due to the large substrate thickness and high refractive index.[2,3,17,35] Here, we access the resonant fringing fields of the metasensor on the top and bottom surfaces by using an ultrathin low refractive index polyimide as the substrate for the metasensor and demonstrate that both of these surfaces could sense the change in the refractive index in its surroundings. The dual sensing surfaces act as dual channels that provide an extra surface for sensing of analytes from the front and rear sides of the metasurface. Moreover, such substrates are extremely flexible and robust in nature, which makes them ideal for potential applications such as wearable sensors.

Although several different unit cell configurations have been proposed for metasensors with respective merits and demerits,[17,18,34,36] the terahertz asymmetric split ring resonator (TASR) has been widely explored with its design freedom and simplicity.[37] A typical TASR design was adopted as the building block of the metamaterial array residing on a flexible polyimide substrate ($n = 1.72$, and the thickness is 25 μm) as schematically shown in Fig. 1(a). Displacing the capacitive gap in the split ring resonator breaks the structural symmetry, resulting in an excitation of the Fano resonance mode, which couples to the *y*-polarized radiation. The properties of the Fano resonance strongly depend on the degree of the asymmetry (d) in TASR.[37] The electric field is confined and enhanced locally in the vicinity of the capacitive gaps of resonators, which thus provides an excellent platform for sensing applications.[4,38,39] In terms of the Fano resonance frequency shift with an analyte film (Germanium, $n = 4.0$), we first performed simulations using commercially available

[a)]Y. K. Srivastava and L. Cong contributed equally to this work.
[b)]Email: ranjans@ntu.edu.sg

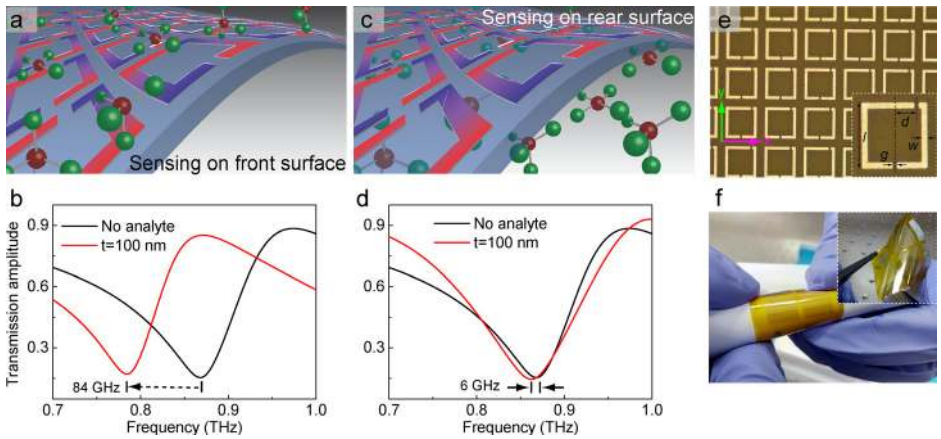

FIG. 1. Dual-surface flexible Fano metasensor. (a) Schematic illustration of sensing from the top surface of the flexible metasensor using a TASR Fano resonator as the building block. (b) Simulated Fano resonance frequency shift with a 100 nm thick analyte (Ge) film. (c) Schematic illustration of sensing from the rear surface of the metasensor. (d) Simulated Fano resonance frequency shift with a 100 nm thick analyte on the bottom surface of the sample. (e) Microscopic image of the fabricated resonator array with geometric parameters of the unit cell shown in the inset as follows: $d = 20$, $w = 6$, $l = 60$, $g = 3$, and a square period of 75 μm. The thickness of the metallic resonators is 200 nm. (f) Images of the fabricated sample showing flexibility and robustness.

software CST Microwave Studio (see supplementary material for details) to show the sensing performance by either depositing the analyte on the top or the bottom of the proposed metasensor surface, as illustrated in Figs. 1(a) and 1(c). The corresponding results are plotted in Figs. 1(b) and 1(d), where we observe a distinct spectral shift of Fano resonance in both scenarios with only a 100 nm thick analyte, exhibiting the dual-surface sensing.

In order to experimentally verify the dual-surface sensing functionality of the metasensor, the sample was fabricated on a 25 μm thick polyimide substrate using conventional photolithography, thermal evaporation of aluminum (200 nm thick), and the lift-off process.[40] The fabricated TASR array is shown in Fig. 1(e). Owing to an excellent flexibility [see Fig. 1(f)], thermal stability, and mechanical strength of the substrate,[41,42] this type of metasensor would have valuable applications in flexible optoelectronic sensing devices.

For refractometric sensing applications, a larger resonance frequency shift is preferred while interacting with the analyte, which thus requires a stronger local field concentration in the volume of the analyte layer according to the perturbation theory[43]

$$\frac{\Delta\omega_i}{\omega_i} = -\frac{1}{2}\frac{\int d\vec{r}\Delta\varepsilon(\vec{r})|E(\vec{r})|^2}{\int d\vec{r}\varepsilon(\vec{r})|E(\vec{r})|^2}, \tag{1}$$

where $\Delta\omega_i$ is the frequency shift of eigenmode i at the resonance frequency ω_i, $\Delta\varepsilon(\vec{r})$ is the change in analyte permittivity, $|E(\vec{r})|$ is the local field intensity, and $\varepsilon(\vec{r})$ is the permittivity of the analyte. Therefore, the refractometric sensitivity ($S = [\Delta\omega_i/(\Delta n_a \times \omega_i)] \times 100\%$, where Δn_a is the change in the analyte refractive index) of a metasensor is proportional to the field flux in the analyte, i.e., $S \propto \int_V |E(\vec{r})|^2 \cdot dV$, where V is volume of the electric field in the analyte.

In this context, we discuss the sensitivity performance of Fano resonance with respect to the metasensor substrate properties. According to the perturbation theory described by Eq. (1), localized field intensity at Fano resonance determines the overall resonance frequency shift with a fixed analyte volume (V). To probe the localized field intensity, we first perform the study through rigorous simulations where a probe was set at the center of the displaced gap in the TASR model, and the electric field intensity was recorded by changing the refractive index of the substrate (n_s) at a fixed thickness of 25 μm. Since the frequency of Fano resonance shifts with the change in n_s, we extracted the localized field intensity at respective resonance (dip) frequencies of the corresponding Fano mode as plotted in Fig. 2(a), where we observe a clear decreasing trend of field intensity with a larger value of the

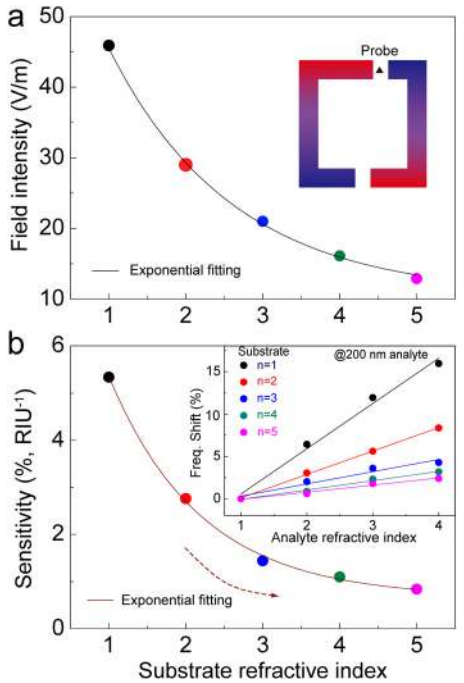

FIG. 2. Sensitivity performance versus refractive index of the metasensor substrate. (a) Localized field intensity at the center of the non-centered gap of TASR at Fano resonance with the substrate of different refractive indices; the inset shows the illustration of the near-field probe of TASR. (b) Retrieved sensitivity ($S = [\Delta\omega_i/(\Delta n \times \omega_i)] \times 100\%$) of the Fano metasensor with the substrate of different refractive indices and exponential decay fitting; the inset shows the linear fit of the frequency shift caused by varying the analyte index ($n = 1$, 2, 3, and 4) at the respective substrate index.

substrate refractive index. An exponential decay of localized electric field amplitude ($|E_l|$) was estimated at the capacitive gap relative to n_s, which is verified by an excellent numerical fit with an equation $|E_l| = 65.1 \cdot e^{-\frac{n_s}{1.6}} + 10.5$ V/m. This exponential decay behavior of the localized electric field determines the resonant frequency shift and sensitivity of the metasensor. We then investigate the refractometric sensitivity (S) of the proposed sensor by depositing a 200 nm thin-film analyte on top of the metallic Fano resonator for different substrate refractive indices, and the sensitivity was retrieved by using a linear fit as shown in the inset of Fig. 2(a). We note that the thickness of the analyte film is around 1/2000 of the operating wavelength at ~0.8 THz ($\lambda = 375\ \mu$m) which is a deep subwavelength regime. The respective sensitivities are plotted in Fig. 2(b), which also reveals a clear exponential decay trend described by an equation $S = 10.8 \cdot e^{-\frac{n_s}{1.2}} + 0.67$ RIU^{-1}. The exponential decay of the sensitivity is similar to the decay of the electric field with an increasing substrate refractive index.

On the basis of the above observations, it is clear that a lower refractive index substrate provides a better thin-film sensitivity. Compared to the commonly used silicon substrate ($n_s = 3.418$),[44] a flexible polyimide ($n_s = 1.72$) is a better candidate for refractometric sensing so as to obtain a large sensitivity. In order to clearly present the contrast of sensitivity between these two configurations, we carried out simulations and experiments using a TASR metamaterial array on two different substrates. Fano resonance spectra were recorded in a dry nitrogen atmosphere, by using a terahertz time-domain spectroscopy (THz-TDS) system in the transmission mode. A normalized transmission amplitude spectrum was obtained by using $|\tilde{t}| = |\tilde{t}_{sam}/\tilde{t}_{ref}|$, where $\tilde{t}_{sam}$ and $\tilde{t}_{ref}$ are the Fourier transformed frequency-domain transmission spectra of the sample and reference (respective bare substrate of different samples, i.e., polyimide and silicon), respectively. Here, we chose to deposit a thin film of semiconductor material Germanium (Ge) as the analyte due to its large refractive index ($n = 4.0$), which provides a relatively large frequency shift. The frequency shift of Fano resonance was clearly observed by depositing different thicknesses of the Ge film on top of the resonator array, and the simulated results are plotted in Fig. 3(a) with 0 nm (without the analyte), 100 nm, 200 nm, and 300 nm Ge thin films on top of the metasensor with polyimide and silicon substrates (inset graph). The Fano frequency shift reveals a distinct contrast in the performance of the metasensors on silicon and polyimide substrates. It is observed that the metasensor on a lower index polyimide substrate gives rise to a much improved and distinguishable frequency shift compared to that on a silicon substrate as shown in the inset of Fig. 3(a). The large resonance frequency shift of the Fano resonator on a polyimide substrate originates from its stronger localized field that enables a larger field flux in an identical thickness of the analyte than that on a silicon substrate. Such a large frequency shift of Fano resonance induced by using a low index polyimide substrate was also verified in experiments as shown in Fig. 3(b), which was found to have a good agreement with the simulated results except for a slight broadening of the resonance linewidth due to larger loss in the experimental metamaterial system. By using a lower index substrate, the sensitivity of a sensor is clearly enhanced so that the resonance frequency shift of an ultrathin film analyte can be easily resolved, which would enhance the application potential of the metasensor in sensing extremely low volumes of biomolecules. So far, we have discussed an enhanced sensitivity performance of the flexible metasensor theoretically and experimentally on the basis of the lower refractive index substrate. As a proof-of-concept, a low index material, polyimide, was adopted for carrying out the experiment. In addition to its advantage of the low refractive index, polyimide also possesses excellent flexibility, robustness, and thermal stability so that such a sensor could be applied in a harsh environment for industrial systems. Its flexibility and robustness also open up another possibility of further enhancing its sensitivity by reducing the substrate thickness which is thinner than the spatial extent of the resonant fringing fields.

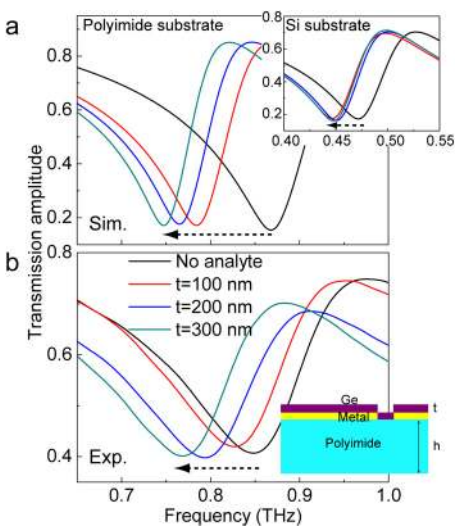

FIG. 3. Experimental demonstration of thin-film sensing from the top surface of the metasensor. (a) Simulated Fano resonance shift by changing the thin-film analyte (Ge) thickness for the metasensor with a polyimide substrate; the inset shows the Fano resonance shift by changing the analyte thickness for the metasensor with a silicon substrate for comparison. (b) Corresponding experimental Fano resonance shift of the metamaterial on a polyimide substrate.

According to the perturbation theory as discussed earlier in Eq. (1), a strengthened localized electric field would give rise to a large resonance frequency shift by changing the refractive index of the surrounding medium. A commonly adopted strategy for sensing is by directly placing the analyte on top of resonators so as to exploit the enhanced local field for a large field flux in the analyte since the fringing field decays spatially above the metasurface. In this sensing scheme, we can only utilize the top surface of the sensor, and the other surface (bottom) becomes redundant due to an optically thick substrate with all the fringing field decaying within the substrate material. In order to access the fringing fields on the rear side of the substrate, the thickness of the substrate must be reduced such that the fields could penetrate through the analyte from the bottom surface (substrate side). However, the commonly adopted rigid thicker substrates hinder the access to the bottom surface fringing fields. A robust, thin, and flexible polyimide substrate overcomes this limitation.

In Fig. 4(a), we show the simulated fringing electric field intensity on both sides of a polyimide based Fano metamaterial sensor at the cut-plane as shown in the inset. The metallic resonators are shown in yellow color, which was

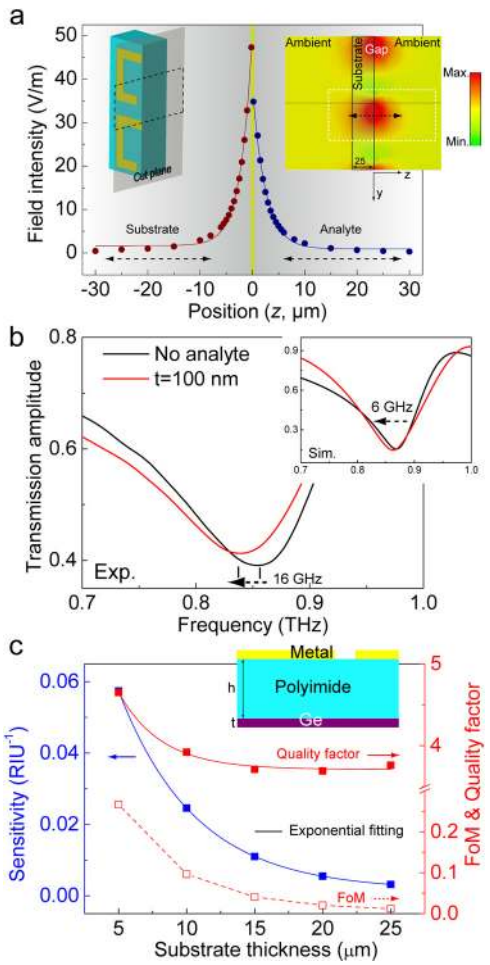

FIG. 4. Spatial extent of fringing fields and bottom surface sensitivity of the flexible metasensor. (a) Spatial distribution of the simulated fringing field on both sides of the metamaterial on a polyimide substrate. (b) Experimental and simulated Fano resonance shift by depositing 100 nm thin-film Ge on the bottom surface of the sample. (c) Investigation of the bottom surface sensitivity by changing the substrate thickness.

considered as an ultrathin film (200 nm) at the zero point of the z axis; the positive axis indicates the free space ambience, and the negative axis indicates the substrate space. As shown in Fig. 4(a), the field intensity on both sides reveals an exponential decay as a function of the spatial extent following $|E_f^n| = 49.0 \cdot e^{\frac{z}{2.2}} + 1.68$ and $|E_f^p| = 37.1 \cdot e^{-\frac{z}{2.5}} + 0.93$ on the negative ($|E_f^n|$) and positive axes ($|E_f^p|$), respectively. The localized field at the metamaterial surface reveals a larger value on the substrate side compared to the free space due to a relatively higher refractive index of the substrate, and consequently, the spatial extent of the fringing field on the substrate side is relatively short, which depends on the refractive index of the substrate. An accessible spatial distribution of the fringing electric field with a low index polyimide substrate enable the detection of the analyte from the bottom surface (substrate side) using the Fano resonance of the metamaterial on a 25 μm thick polyimide substrate. As shown in Fig. 4(b), we measured the frequency shift of the Fano resonance with 100 nm Ge deposited on the substrate side of the metasensor, which is also verified by the simulated results shown in the inset. Thus, the dual-surface sensing is enabled by the polyimide substrate based metasensors.

A detailed study of the bottom surface sensing is performed using rigorous simulations by varying the polyimide substrate thickness. As per the exponential decay of the spatial electric field, a thinner substrate provides a larger bottom surface sensitivity for the analyte deposited on the bottom surface of the *substrate* as indicated by the blue line in Fig. 4(c). The quality factor of Fano resonance also increases by decreasing the substrate thickness due to reduced dissipation in the lossy substrate. A Figure of Merit (FoM) parameter, calculated by $FoM = S \times Q$, where S is the sensitivity and Q is the quality factor, indicates the overall sensing performance. The calculated FoM values of Fano sensors with a polyimide substrate at different thicknesses are also depicted in Fig. 4(c), and it is clearly seen that the sensitivity is enhanced in the case of thinner substrates. Our metasensor design consists of a lower quality factor resonance due to the limited energy confinement in the low-index substrate and the large amplitude of the Fano resonance. Fano resonances are weakly coupled to the free space and have extremely low resonance amplitude, which pose the challenge in performing accurate measurements. Therefore, we enhanced the asymmetry of the structure to excite a strong Fano resonance which typically results in the broadening of its linewidth and a decline in the Q factor.[37]

We further simulated the resultant Fano resonance shift by depositing analyte on the top and bottom surfaces with a 100 nm thin-film of Germanium. As shown in Fig. 5(a), it is visible that the total frequency shift of Fano resonance is enhanced to 89 GHz. The total resonance shift is almost the sum of the shift caused by individual surfaces (top: 84 GHz and bottom: 6 GHz), which demonstrates the effect of an additional sensing channel (surface).

The application of sensors on irregular surfaces of three-dimensional objects is quite important. Thus, we also

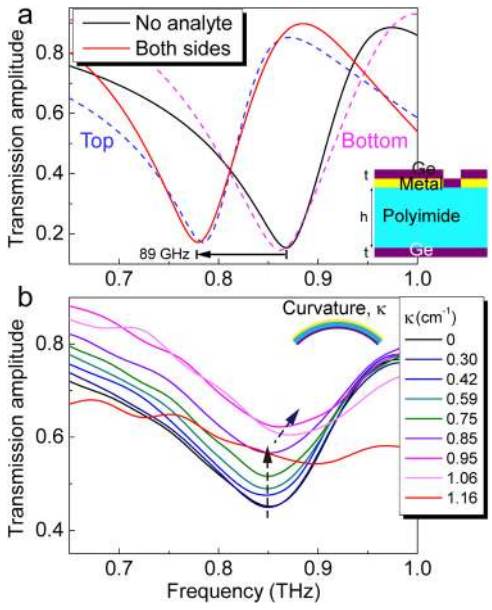

FIG. 5. Resonance shift by coating the analyte on both surfaces and the flexibility test of the flexible metasensor. (a) Simulated Fano resonance shift with a 100 nm analyte on both top and bottom surfaces of the flexible metasensor. Dashed lines show the Fano spectra for the metasensor with the analyte only on top (blue) and bottom surfaces (pink) for comparison. (b) Measured Fano spectra of the metasensor at different curvatures.

performed the flexibility test on our metasensor at different curvatures (κ, $\kappa = 1/R$, where R is the radius of the curved sample, see supplementary material) and measured the spectral responses as shown in Fig. 5(b). We observe a stable Fano resonance frequency response with a slight modulation in the transmission amplitude when the curvature is less than $0.85\,\mathrm{cm}^{-1}$. The stability of Fano resonance frequency starts to deteriorate when curvature exceeds $0.85\,\mathrm{cm}^{-1}$ since the resonator geometry, the array uniformity, and the density of resonators get affected at larger curvature. The proposed dual-surface metasensor would be a good candidate as a 3D flexible sensor which could find practical applications.

In summary, we have experimentally demonstrated a dual-surface terahertz metasensor on an ultrathin flexible substrate with a low refractive index that reveals a highly enhanced sensitivity. The ultrathin, low index, and flexible design of the metasensor enables sensing of the analyte from the top and bottom surfaces of the metamaterial. This flexible Fano sensor would open up a broader range of applications in industrial sensing systems and enable an enhanced performance in biosensing with a lower molecule concentration. Such a sensor scheme could also to be extended into different sensing configurations as per the on-demand applications.

See supplementary material for the information on the simulation methods and sample flexibility test.

The authors thank the Singapore Ministry of Education Grant No. MOE2015-T2-2-103 for funding of this research.

[1]P. H. Siegel, IEEE Trans. Microwave Theory Tech. **52**(10), 2438–2447 (2004).
[2]J. N. Anker, W. P. Hall, O. Lyandres, N. C. Shah, J. Zhao, and R. P. Van Duyne, Nat. Mater. **7**(6), 442–453 (2008).
[3]H. Im, H. Shao, Y. I. Park, V. M. Peterson, C. M. Castro, R. Weissleder, and H. Lee, Nat. Biotechnol. **32**(5), 490–495 (2014).
[4]C. Wu, A. B. Khanikaev, R. Adato, N. Arju, A. A. Yanik, H. Altug, and G. Shvets, Nat. Mater. **11**(1), 69–75 (2012).
[5]W. Withayachumnankul, G. M. Png, X. Yin, S. Atakaramians, I. Jones, H. Lin, B. S. Y. Ung, J. Balakrishnan, B. W. H. Ng, B. Ferguson, S. P. Mickan, B. M. Fischer, and D. Abbott, Proc. IEEE **95**(8), 1528–1558 (2007).
[6]J. Chen, Y. Chen, H. Zhao, G. J. Bastiaans, and X.-C. Zhang, Opt. Express **15**(19), 12060–12067 (2007).
[7]B. Fischer, M. Walther, and P. U. Jepsen, Phys. Med. Biol. **47**(21), 3807 (2002).
[8]Y. Shvyd'Ko, *X-Ray Optics: High-Energy-Resolution Applications* (Springer, 2013).
[9]X.-C. Zhang and J. Xu, *Introduction to THz Wave Photonics* (Springer, 2010).
[10]D. R. Smith, J. B. Pendry, and M. C. Wiltshire, Science **305**(5685), 788–792 (2004).
[11]Y. Chen, I. A. I. Al-Naib, J. Gu, M. Wang, T. Ozaki, R. Morandotti, and W. Zhang, AIP Adv. **2**(2), 022109 (2012).
[12]L. Xie, W. Gao, J. Shu, Y. Ying, and J. Kono, Sci. Rep. **5**, 8671 (2015).
[13]W. Xu, L. Xie, and Y. Ying, Nanoscale **9**(37), 13864–13878 (2017).
[14]M. Chen, L. Singh, N. Xu, R. Singh, W. Zhang, and L. Xie, Opt. Express **25**(13), 14089–14097 (2017).
[15]M. Gupta, Y. K. Srivastava, M. Manjappa, and R. Singh, Appl. Phys. Lett. **110**(12), 121108 (2017).
[16]L. Cong, S. Tan, R. Yahiaoui, F. Yan, W. Zhang, and R. Singh, Appl. Phys. Lett. **106**(3), 031107 (2015).
[17]N. Liu, M. Mesch, T. Weiss, M. Hentschel, and H. Giessen, Nano Lett. **10**(7), 2342–2348 (2010).
[18]N. Liu, T. Weiss, M. Mesch, L. Langguth, U. Eigenthaler, M. Hirscher, C. Sönnichsen, and H. Giessen, Nano Lett. **10**(4), 1103–1107 (2010).
[19]A. Kabashin, P. Evans, S. Pastkovsky, W. Hendren, G. Wurtz, R. Atkinson, R. Pollard, V. Podolskiy, and A. Zayats, Nat. Mater. **8**(11), 867–871 (2009).
[20]N. Born, I. Al-Naib, C. Jansen, R. Singh, J. V. Moloney, M. Scheller, and M. Koch, Adv. Opt. Mater. **3**(5), 642–645 (2015).
[21]Y. Yang, I. I. Kravchenko, D. P. Briggs, and J. Valentine, Nat. Commun. **5**, 5753 (2014).
[22]A. I. Kuznetsov, A. E. Miroshnichenko, M. L. Brongersma, Y. S. Kivshar, and B. Luk'yanchuk, Science **354**(6314), aag2472 (2016).
[23]A. Ebrahimi, W. Withayachumnankul, S. Al-Sarawi, and D. Abbott, IEEE Sens. J. **14**(5), 1345–1351 (2014).
[24]I. A. I. Al-Naib, C. Jansen, and M. Koch, Appl. Phys. Lett. **93**(8), 083507 (2008).
[25]I. Al-Naib, IEEE J. Sel. Top. Quantum Electron. **23**(4), 1–5 (2017).
[26]B. Reinhard, K. M. Schmitt, V. Wollrab, J. Neu, R. Beigang, and M. Rahm, Appl. Phys. Lett. **100**(22), 221101 (2012).
[27]J. A. Rogers, T. Someya, and Y. Huang, Science **327**(5973), 1603–1607 (2010).
[28]D.-H. Kim, N. Lu, R. Ma, Y.-S. Kim, R.-H. Kim, S. Wang, J. Wu, S. M. Won, H. Tao, A. Islam, K. J. Yu, T.-i. Kim, R. Chowdhury, M. Ying, L. Xu, M. Li, H.-J. Chung, H. Keum, M. McCormick, P. Liu, Y.-W. Zhang, F. G. Omenetto, Y. Huang, T. Coleman, and J. A. Rogers, Science **333**(6044), 838–843 (2011).
[29]T. Aernouts, P. Vanlaeke, W. Geens, J. Poortmans, P. Heremans, S. Borghs, R. Mertens, R. Andriessen, and L. Leenders, Thin Solid Films **451–452**, 22–25 (2004).
[30]H. Tao, L. R. Chieffo, M. A. Brenckle, S. M. Siebert, M. Liu, A. C. Strikwerda, K. Fan, D. L. Kaplan, X. Zhang, R. D. Averitt, and F. G. Omenetto, Adv. Mater. **23**(28), 3197–3201 (2011).
[31]L. Cong, Y. K. Srivastava, A. Solanki, T. C. Sum, and R. Singh, ACS Photonics **4**(7), 1595–1601 (2017).
[32]A. Sadeqi, H. R. Nejad, and S. Sonkusale, Opt. Express **25**(14), 16092–16100 (2017).
[33]R. Yahiaoui, S. Tan, L. Cong, R. Singh, F. Yan, and W. Zhang, J. Appl. Phys. **118**(8), 083103 (2015).
[34]H. Tao, A. C. Strikwerda, M. Liu, J. P. Mondia, E. Ekmekci, K. Fan, D. L. Kaplan, W. J. Padilla, X. Zhang, R. D. Averitt, and F. G. Omenetto, Appl. Phys. Lett. **97**(26), 261909 (2010).
[35]K. V. Sreekanth, Y. Alapan, M. ElKabbash, E. Ilker, M. Hinczewski, U. A. Gurkan, A. De Luca, and G. Strangi, Nat. Mater. **15**(6), 621–627 (2016).
[36]E. Cubukcu, S. Zhang, Y.-S. Park, G. Bartal, and X. Zhang, Appl. Phys. Lett. **95**(4), 043113 (2009).
[37]L. Cong, M. Manjappa, N. Xu, I. Al-Naib, W. Zhang, and R. Singh, Adv. Opt. Mater. **3**(11), 1537–1543 (2015).
[38]B. Luk'yanchuk, N. I. Zheludev, S. A. Maier, N. J. Halas, P. Nordlander, H. Giessen, and C. T. Chong, Nat. Mater. **9**(9), 707–715 (2010).
[39]R. Singh, W. Cao, I. Al-Naib, L. Cong, W. Withayachumnankul, and W. Zhang, Appl. Phys. Lett. **105**(17), 171101 (2014).
[40]S. Walia, C. M. Shah, P. Gutruf, H. Nili, D. R. Chowdhury, W. Withayachumnankul, M. Bhaskaran, and S. Sriram, Appl. Phys. Rev. **2**(1), 011303 (2015).
[41]W. A. MacDonald, M. K. Looney, D. MacKerron, R. Eveson, R. Adam, K. Hashimoto, and K. Rakos, J. Soc. Inf. Disp. **15**(12), 1075–1083 (2007).
[42]W. A. MacDonald, J. Mater. Chem. **14**(1), 4–10 (2004).
[43]W. Zhang and O. J. F. Martin, ACS Photonics **2**(1), 144–150 (2015).
[44]J. Dai, J. Zhang, W. Zhang, and D. Grischkowsky, J. Opt. Soc. Am. B **21**(7), 1379–1386 (2004).